Proceedings of
11th European Conference on Turbomachinery Fluid dynamics & Thermodynamics
ETC11, March 23-27, 2015, Madrid, Spain

PROBABILISTIC ANALYSIS OF MANUFACTURING UNCERTAINTIES FOR AN AUTOMOTIVE TURBOCHARGER CENTRIFUGAL COMPRESSOR USING NUMERICAL AND EXPERIMENTAL METHODS

A. Javed[1], *E. Kamphues*

Mitsubishi Turbocharger and Engine Europe BV
The Netherlands
Email: adeel.javed@epfl.ch, ekamphues@mtee.eu

T. Hartuc, R. Pecnik, J. P. van Buijtenen

Delft University of Technology
The Netherlands
Email: t.hartuc@student.tudelft.nl, r.pecnik@tudelft.nl, j.p.vanbuijtenen@tudelft.nl

ABSTRACT

The compressor impellers for mass-produced turbochargers are generally die-casted and machined to their final configuration. Manufacturing uncertainties are inherently introduced as stochastic dimensional deviations in the impeller geometry. These deviations eventually propagate into the compressor functionality as variability in output performance. This paper presents a probabilistic evaluation of the impact of manufacturing uncertainties on the compressor performance using the non-intrusive Monte Carlo method coupled with metamodels prepared for compressor performance modeling using computational fluid dynamics (CFD) and comprehensive experimentation. The probabilistic evaluation or the uncertainty quantification (UQ) of manufacturing uncertainties has identified the most sensitive and uncertain of the impeller geometric parameters contributing the most to variability in compressor performance. Consequently, the tolerances of different impeller dimensions can be reviewed, thereby influencing the production quality and costs.

NOMENCLATURE

Symbols		**Subscripts**	
b	Height [mm]	1	Impeller inlet
D	Diameter [mm]	2	Impeller outlet
r	Radius [mm]	5	Diffuser exit
R^2	Coefficient of determination	7	Volute outlet
t	Thickness, Tip-clearance [mm]	*adj*	Adjusted
y^+	Non-dimensional distance [-]	*b*	Blade
Z	Blade number [-]	*clr*	Clearance
Greek Symbols		*s*	Shroud
β	Relative angle [^{o}]	*t*	Tip
μ	Mean		
η	Efficiency [%]		
Π	Pressure Ratio [-]		
σ	Standard Deviation		

[1] Currently at École Polytechnique Fédérale de Lausanne (EPFL), CH-1015 Lausanne, Switzerland.

INTRODUCTION

Manufacturing processes introduce systematic and random deviations in part geometry due to inherent manufacturing uncertainties. These manufacturing uncertainties are the errors which can be caused by any aspect of a manufacturing process such as geometric errors in the production machines, wear in the cutting tools, human error, etc. The manufacturing uncertainties propagate to part performance as an undesirable variation. Therefore, a validated quantification of the influence of manufacturing uncertainties on part performance is valuable.

Several studies have been performed on axial turbomachinery to quantify the effects of manufacturing uncertainties on performance using probabilistic techniques. Effects of manufacturing tolerances on axial turbine cooling have been presented in (Bunker, 2009). A probabilistic methodology using principal-component analysis (PCA) based blade geometry model coupled with a quasi-2D blade-passage analysis tool has been defined in ref. (Gazron and Darmofal, 2003) to optimize compressor airfoils with 30% to 40% lower variability in efficiency. Similar studies have been performed in ref. (Lecerf et al, 2003, Bestle et al, 2010, Kumar et al, 2008) using a metamodel based robust optimization of axial compressor blades. However, all these case studies have been performed on simplified 2D airfoil sections without experimental validation.

Automotive turbochargers are produced in millions every year. Such machines have miniature dimensions and tolerance specifications compared to their larger equivalents. For a turbocharger compressor, a number of manufacturing processes are involved in its production, all of which can induce dimensional deviations caused by the manufacturing uncertainties. The impellers in particular, are generally manufactured by aluminum die casting process (Sotome and Sakoda, 2007) with subsequent machining of the raw impeller castings to their final configuration. The impeller castings are also trimmed using appropriate machining to achieve different flow capacities and pressure heads by removing excess material from the impeller blade tips. Manufacturing uncertainty quantification for a turbocharger application focusing on the impeller is, therefore, very valuable since the procedure can lead to the identification and removal of unnecessarily strict tolerances, tolerance relaxation for difficult dimensions and an overall reduction in manufacturing costs.

METHODOLOGY

For the turbocharger compressor under focus, a three-step generic methodology has been applied to perform the manufacturing uncertainty quantification. A parameter-wise sensitivity evaluation is first performed to determine how the variability in an output quantity of interest is connected to the input in a system. A sensitivity ranking is finally built to identify the most sensitive input parameters, dominating the system response. The sensitivity analysis is followed by the UQ, which measures the variability in the output caused by the presence of stochastic uncertainties in the inputs. The non-intrusive Monte Carlo method (Hurtado and Barbat, 1998) has been used for uncertainty propagation by simulating the random manufacturing uncertainties. Statistical evaluation of the output performance is performed to determine the output mean and variability either as standard deviation or variance. Finally the analysis of variance (ANOVA) identifies the most uncertain input parameters by decomposing the variance in a measured outcome to the input sources. Suitable experimental information is required for validating the outcomes from a model in order to achieve a reasonable assurance of its predictive accuracy. As a final step, the computational UQ has been experimentally validated by testing a selected number of impellers on a turbocharger test bench at Mitsubishi Turbocharger and Engine Europe BV (MTEE).

TURBOCHARGER COMPRESSOR TEST CASE

The test case turbocharger compressor comprises of an impeller wheel, a vaneless diffuser and an overhung type volute as shown in Fig. 1 along with some of the geometric specifications provided in Table 1. The impeller is designed with backswept full and splitter blades, six each in number. The vaneless diffuser uses a shroud pinch. The diffuser flow is finally collected in the overhung volute, thereby completing the compressor stage.

Figure 1 – The test case turbocharger compressor

Table 1 – Geometric specifications of the turbocharger compressor

Component	Parameter	Dimension
Impeller	Inlet shroud radius, r_{1s} [mm]	13.1
	Tip radius, r_2 [mm]	18.5
	Tip height, b_2 [mm]	2.6
	Blade thickness, t_b [mm]	0.5
	Number of blades, Z [-]	12
	Backsweep angle, β_{2b} [deg]	35
Vaneless diffuser	Outlet radius, r_5 [mm]	33
	Outlet height, b_5 [mm]	1.7
Volute	Outlet diameter, D_7 [mm]	27.5

Generally, the operating or dynamic tip-clearance is smaller than the stationary tip-clearance. The clearance gap between the impeller and the shroud cover reduces due to radial and axial displacement of the impeller, caused by centrifugal effects and shaft movement. For the test case compressor, the operating tip-clearance was unknown. Therefore, an approximated operating tip-clearance of 6% of the impeller tip height b_2 estimated by a CFD evaluation (Olivero et al, 2011) has been used for the analysis.

COMPRESSOR PERFORMANCE MODELING

In order to carry out the probabilistic evaluation using the Monte Carlo method, a computationally inexpensive and reasonably accurate compressor performance model is required. Metamodels have been constructed therefore, through a comprehensive design of experiments (DoE) conducted in CFD for swift compressor performance calculations.

DoE for the Test Case Impeller

The technique of defining and investigating the possible conditions in an experiment or trial calculations involving multiple design variables is known as DoE (Shahpar, 2004). The objective of DoE in such a context is to generate a data that can be used to fit a metamodel, which reliably predicts the true trends of the input-output relationship (Keane and Nair, 2005). Latin hypercube sampling (LHS), a well-known and widely used space-filling DoE method, has been applied as the DoE method for the test case impeller. The underlying concept of LHS sampling method is to divide the design space into a number of bins of equal probability and generate pseudo random samples, such that for each design variable, no two design points lie in the same bin. A total of 200 LHS designs have been employed. All the DoE samples have been parameterized and simulated in CFD at the best-efficiency operating point, i.e., 60g/s mass flow rate at 220,000rpm rotational speed.

Impeller Parameterization for DoE

For the turbocharger compressor, the available geometric data in shape of part drawings and physical measurements have been transformed into a 3D geometric model using the commercial software ANSYS BladeGen. The parameterization of the compressor is shown in Fig. 2(a). The inlet duct, impeller and the vaneless diffuser have been modeled as a single passage fluid domain. The impeller hub and shroud profiles have been converted to third-order Bézier curves, which provide an adequate resolution and control of the impeller shape. The variation in geometry and Bézier control points has been restricted to a single

Table 2 – Selected impeller geometric parameters and their deviations

Parameter	Deviation	Lower	Nominal	Upper
Inducer tip-clearance, $t_{clr,1}$ [mm]	±0.1	0.05	0.15	0.25
Exducer tip-clearance, $t_{clr,2}$ [mm]	±0.1	0.05	0.15	0.25
Inlet hub radius, r_{1h} [mm]	±0.2	4.6	4.8	5.0
Tip radius, r_2 [mm]	±0.5	18.0	18.5	19.0
Blade thickness, t_b [mm]	±0.1	0.4	0.5	0.6
Inlet blade angle at tip*, β_{1bt} [deg]	±2°	63°	65°	67°
Backsweep angle, β_{2b} [deg]	±2°	33°	35°	37°

∗ similar deviation is applied to inlet blade angles at mid-span and hub

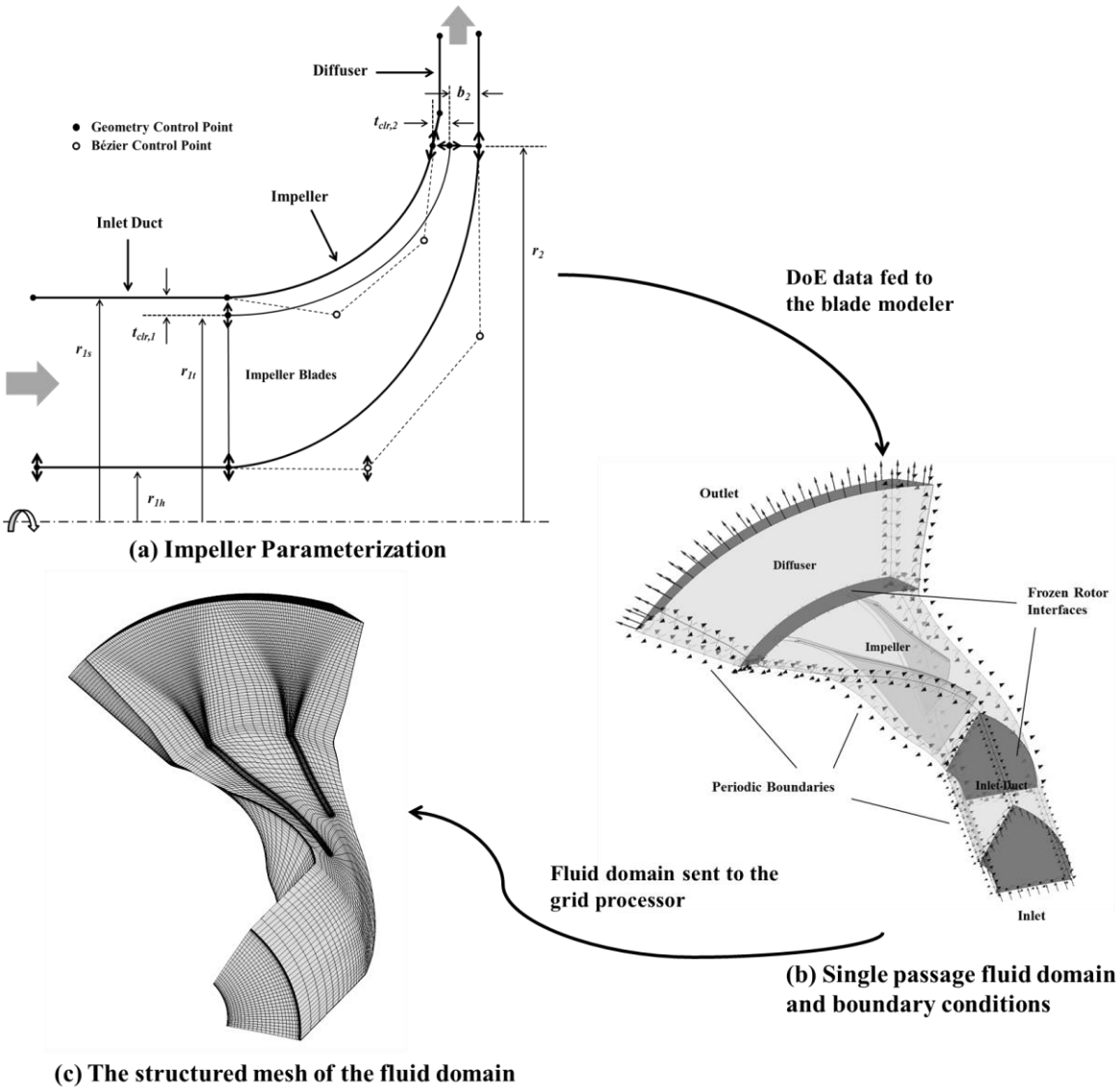

Figure 2 – Illustration of the preprocessing for impeller DoE using CFD

dimension. The blade thickness has been assumed constant from hub to shroud while the volute has been excluded to reduce the computational expense. Seven main impeller geometric parameters have been selected and assigned a hypothetical deviation range as given in Table 2 in order to define the DoE design space. Manufacturing deviations introduced during impeller trimming will ultimately vary the tip-clearance gaps between the impeller and the constant shroud cover. Therefore, the deviations in the inlet tip radius r_{1t} and exducer height b_2 have been modeled as the inducer tip-clearance $t_{clr,1}$ and exducer tip-clearance $t_{clr,2}$. The geometry of the impeller shroud cover formed by the compressor housing has been maintained constant to focus on the influence of manufacturing deviations in the impeller only. Finally, the impeller blade shape is controlled by the inlet blade angles β_{1b} and the backsweep angle β_{2b}. The remaining blade shape is kept constant.

CFD Preprocessing and Solution Setup

Grid Processing

A 3D structured grid has been created in ANSYS TurboGrid using the H-Grid and O-Grid topologies as illustrated in Fig. 2(c). The O-Grid topology provides a good mesh around the blades, while rest of the passage consists of the H-Grid. The mesh at the inlet-impeller and impeller-diffuser interfaces is conformal, i.e., the grid is shared between the two connecting surfaces at the

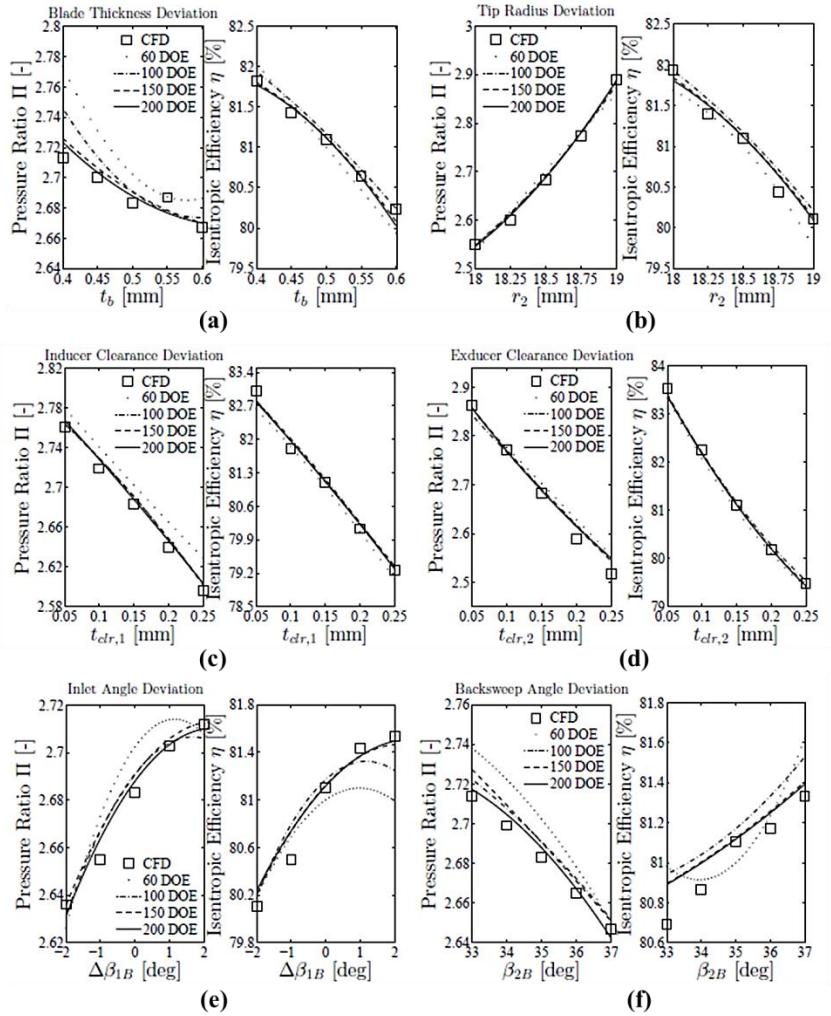

Figure 3 – Performance evaluation of impeller geometric deviations using the response surface and comparison with the CFD data

interface. The grid downstream of the impeller blades into the diffuser is also well resolved thus facilitating a good modeling of downstream blade wakes. The near-wall mesh has been made fine by providing sufficient number of nodes in the boundary layer region. As a result, an overall *y+* approximately equal to 1 has been achieved at the wall boundaries except the TE of the blades, where a fine near-wall mesh could not be constructed. The tip-clearance gap of 0.15mm (approximately 6% of tip height b_2) is introduced in TurboGrid by trimming down the blade shroud profile. The number of hexahedral elements in the clearance gap has been set to 15 to capture the clearance gap flow and associated properties.

A grid independence study has been performed at the best-efficiency operating point using three different grid sizes of 0.25 million, 0.475 million and 0.70 million hexahedral elements. Impeller and diffuser outlet properties including pressure ratio and efficiency have been compared for the three grid sizes. Maximum difference in pressure ratio and isentropic efficiency has been found to be approximately 0.18% and 0.15% respectively for the three grid sizes. Based on this marginal variation in properties with increasing grid size, the intermediate grid of 0.475 million elements is selected for further modeling.

Boundary Conditions

Figure 2(b) also illustrates the different boundary conditions applied to the compressor fluid domain. Periodic boundary conditions are defined at the symmetric surfaces by assuming the fluid properties to be periodically repetitive (especially near the best-efficiency operating point). The

impeller shroud has been defined as a counter-rotating wall. The compressor walls have been assumed to be hydraulically smooth. At the compressor inlet, total temperature and total pressure of 288.15K and 101.325kPa, respectively, have been defined, which correspond to the International Standard Atmosphere (ISA) ambient conditions. In addition, a medium turbulent intensity of 5% has been maintained at the inlet boundary for all compressor simulations. Different mass flow rates have been defined at the outlet boundary condition to simulate the compressor speed line. However, close to choke, where slightest variations in mass flow can result in a considerable change in performance, static pressure has been defined. Finally, the interfaces between the inlet duct, impeller and the vaneless diffuser are defined as frozen rotor.

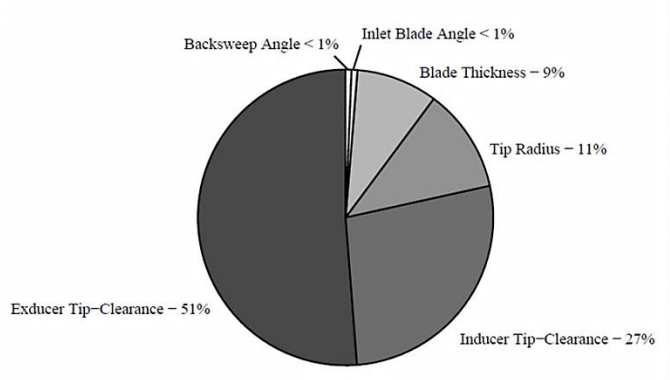

(a) Pressure Ratio

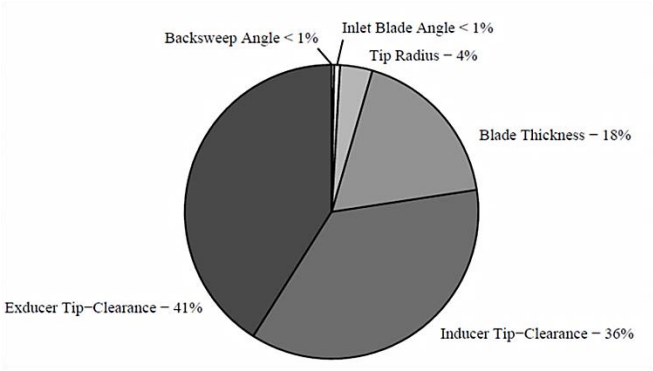

(b) Isentropic Efficiency

Figure 4 – Sensitivity ranking of impeller performance due to geometric deviations predicted by the response surface models

Turbulence Model Selection

The widely used k-ω Shear Stress Transport (SST) turbulence model (Menter, 1993) has been applied for the CFD simulations of the test case turbocharger compressor.

Metamodel for the Test Case Impeller

Metamodels are constructed using the DoE data drawn from high-fidelity models, and provide fast approximations of the function values at new design points. Many kinds of metamodels are available. For this study, the polynomial response surface model (Meyers and Montgomery, 1995) has been selected as the metamodel for impeller performance prediction.

Two quadratic response surface models, each for the impeller pressure ratio and isentropic efficiency were constructed over the DoE responses. To check the model fit, coefficient of correlation R^2 and the adjusted R^2_{adj} statistical tests are used. With 200 LHS designs the response surface for the pressure ratio resulted in R^2 and R^2_{adj} to be 0.989 and 0.975 respectively. This indicates that the model can capture about 98.9% and 97.5% of the variability respectively in predicting new observations. For the impeller efficiency response surface, R^2 and R^2_{adj} are 0.977 and 0.945 respectively, which also reveals that the model can mimic 97.7% and 94.5% of the variability respectively in predicting new observations. The high values for the coefficient of correlations from 0.9 to 1.0 indicate a good model fit.

Figure 3 shows a comparison between the outcomes from the two response surface models constructed for different sample sizes, and compared with the corresponding CFD data. The hub radius r_{1h} has been excluded from the analysis due to its negligible influence on impeller performance. Interestingly, as the number of DoE samples increases from 60 to a maximum of 200, the predictions made by response surface models gradually improve in accuracy. As convergence is achieved, the response surface models have successfully emulated the CFD data and are now capable to predict impeller performance at new observations.

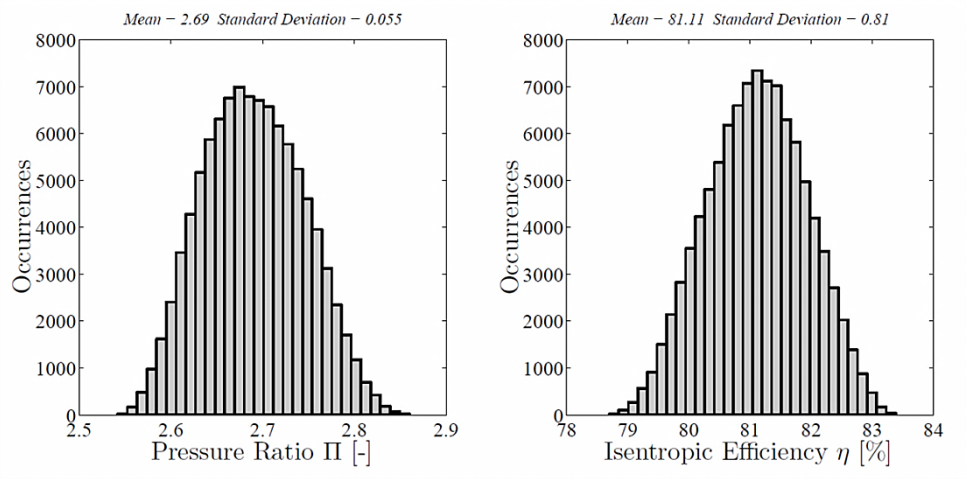

Figure 5 – Probability distributions of variation in impeller pressure ratio and isentropic efficiency predicted by the metamodel based Monte Carlo simulation

SENSITIVITY ANALYSIS AND PARAMETER-WISE RANKING

In addition to presenting the metamodel convergence, Fig. 3 also illustrates the sensitivity of impeller pressure ratio and isentropic efficiency as a function of different geometric parameters. The results have been used to determine the sensitivity derivatives $\partial q/\partial \xi$ for each input parameter by calculating the ratio of the total variation in the output quantity of interest q to the total deviation in the input ξ for the predefined deviation range given in Table 2. Figure 4 summarizes the impeller pressure ratio and isentropic efficiency sensitivities as percentages. Evidently, the inducer tip-clearance $t_{clr,1}$ and the exducer tip-clearance $t_{clr,2}$ are contributing the most to impeller performance variation, while blade thickness t_b and tip radius r_2 are also sensitive geometric parameters. In comparison, the remaining geometric parameters have a marginal influence on impeller performance. Therefore, based on the sensitivity ranking, the inducer tip-clearance $t_{clr,1}$, exducer tip-clearance $t_{clr,2}$, along with the blade thickness t_b and the tip radius r_2 have been selected for further analyses as the most sensitive impeller geometric parameters.

MANUFACURING UNCERTAINTY QUANTIFICATION

To propagate the manufacturing uncertainties using Monte Carlo method, suitable tolerances have been defined for the sensitive geometric parameters as given in Table 3. Actual manufacturing tolerances for the impeller cannot be disclosed due to confidentiality. Uniform probability distribution has been assumed for defining the input parameter variability. It is the simplest type in which all the quantities of a random input variable occur with equal probability. As a consequence, the computed results can be considered as conservative estimates of the actual predictions. A total of hundred thousand Monte Carlo samples have been simulated using the metamodels. The results have been used to calculate the mean μ and standard deviation σ of impeller pressure ratio and isentropic efficiency. The impeller pressure ratio and isentropic efficiency exhibit normal or Gaussian probability distributions as shown in Fig 5. The mean and standard deviation of impeller pressure ratio are 2.69 and 0.055, respectively, while the mean and standard deviation of impeller

Table 3 – Sensitive impeller geometric parameters and their tolerances

Parameter	Deviation	Lower	Nominal	Upper
Inducer tip clearance, $t_{clr,1}$ [mm]	±0.05	0.1	0.15	0.2
Exducer tip clearance, $t_{clr,2}$ [mm]	±0.05	0.1	0.15	0.2
Tip radius, r_2 [mm]	±0.1	18.4	18.5	18.6
Blade thickness, t_b [mm]	±0.05	0.45	0.5	0.55

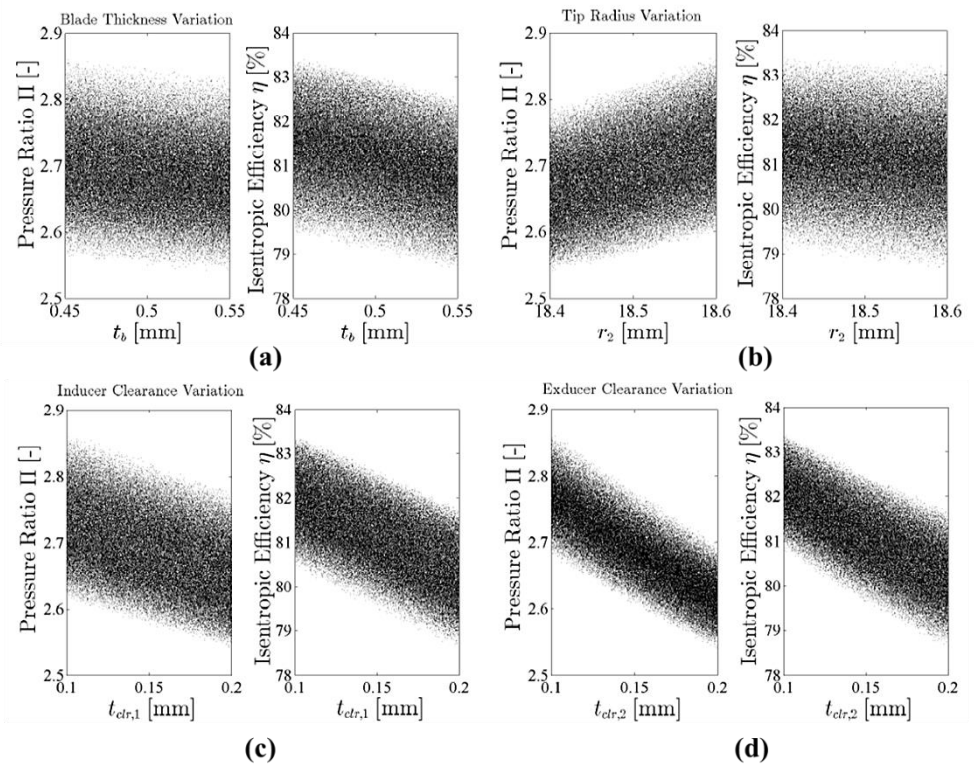

Figure 6 – Scatter plots from Monte Carlo simulation showing the effects of geometric variation on impeller performance

isentropic efficiency are 81.11% and 0.81, respectively. The resulting variation in pressure ratio ranges approximately from 2.53 to 2.85, while isentropic efficiency ranges from 78.69% to 85.53%, equally covering $\pm 3\sigma$ normal distributions.

The data from the Monte Carlo simulation has been used to perform the analysis of variance (ANOVA) to identify the most uncertain impeller geometric parameters. Figure 6 shows the scatter plots of impeller performance variation. The impeller pressure ratio and isentropic efficiency, predicted by their respective response surface models, have been plotted against the sensitive impeller geometric parameters. Consider Fig. 6(a), which shows the impeller performance scatter for blade thickness t_b. For a fixed value of t_b, the scatter observed in impeller performance is being caused by the uncertainty introduced from the rest of the geometric parameters. The plot hence shows that the uncertainty in impeller performance is large, but the contribution of t_b to this uncertainty is insignificant. In comparison, the scatter plot given in Fig. 6(d) for exducer tip-clearance $t_{clr,2}$ shows a large contribution of the geometric parameter to uncertainty in impeller performance. The sum of squares due to regression SS_R, partitioned for each of the impeller geometric parameters, and the sum of squares due to error SS_E have been used to evaluate and rank the sources of variance. Uncertainty ranking of impeller geometric parameters is shown in Fig. 7. The inducer tip-clearance $t_{clr,1}$ and the exducer tip-clearance $t_{clr,2}$ are contributing the most to impeller performance uncertainty. The tip radius r_2 has more influence on uncertainty in pressure ratio, while having a marginal contribution to uncertainty in impeller isentropic efficiency. Conversely, uncertainty in impeller pressure ratio has a marginal contribution from t_b, while it has a considerable influence on uncertainty in impeller isentropic efficiency. Lastly, the sum of squares due to error SS_E related to model fit has a negligible impact on overall performance uncertainty. ANOVA has suggested that $t_{clr,1}$ and $t_{clr,2}$ are the most critical parameters due to their considerable influence on overall impeller performance.

EXPERIMENTAL VALIDATION

The computational UQ has been validated through a comprehensive experimentation at MTEE turbocharger testing facility.

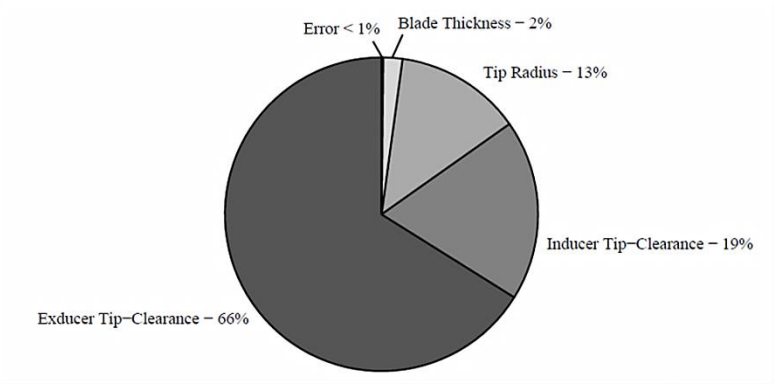

(a) Pressure Ratio

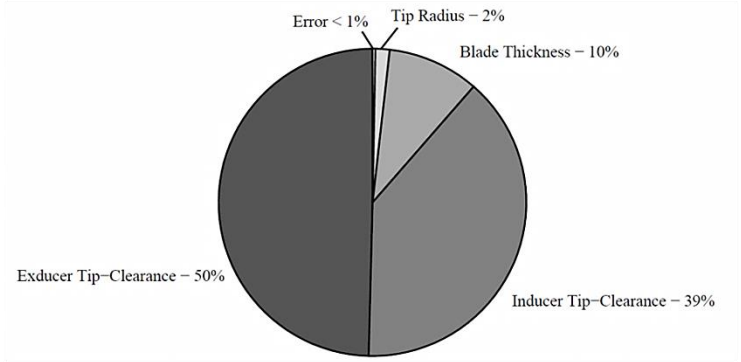

(b) Isentropic Efficiency

Figure 7 – Uncertainty ranking of impeller geometric parameters decomposed by ANOVA

DoE for the Test Case Impeller

Compared to a computational DoE, an experimental DoE is expensive to build and execute. Therefore, three impeller geometric parameters have been considered due to their importance and ease of manufacture − the inducer tip-clearance $t_{clr,1}$, exducer tip-clearance $t_{clr,2}$ and the tip radius r_2. The remaining geometric parameters are unchanged and maintained at their nominal values.

A 3^k full-factorial design (Meyers and Montgomery, 1995) consisting of all the combinations of k number of design variables having three levels each, has been used for the experimental DoE. With three geometric parameters considered for DoE, this corresponds to $3^3 = 27$ unique design combinations, where a third level facilitates the evaluation of a quadratic input-output relationship. Table 4 shows the selected deviation range for the three geometric parameters. The repeatability or stability of the experiments has to be determined to quantify the measurement uncertainties. Hence, a total of five center point measurements have been carried out using a single impeller having the nominal geometry. All in all, a total of 32 tests have been made for the experimental DoE.

The steady-state tip-clearances[2] at the inducer and the exducer sections are expected to reduce up to 6% of exducer height b_2 during turbocharger operation at high rotational speeds, thereby complying with the operating tip-clearance values used in the computational DoE. Therefore, the selected deviation has been introduced in the steady-state tip-clearances for the impeller and machined accordingly.

Manufacturing of DoE Impellers

The manufacturing process of the DoE impellers consists of three main stages. First the impellers have been acquired as raw castings as shown in Fig. 8(a). In the second and third stages, the castings undergo turning operations in the computer numerical control (CNC) lathe machine. Figure 8(b) shows the impellers after the second stage machining operation. The third stage machining operation forms the shroud profile of the impeller blades as shown in Fig. 8(c). The

Table 4 – Selected impeller geometric parameters and their deviations

Parameter	Deviation	Lower	Nominal	Upper
Inducer tip-clearance*, $t_{clr,1}$ [mm]	±0.1	-	-	-
Exducer tip-clearance*, $t_{clr,2}$ [mm]	±0.1	-	-	-
Tip radius, r_2 [mm]	±0.5	18.0	18.5	19.0

∗ confidential information

[2] The information on the nominal steady-state tip-clearance values and the respective lower and upper deviations cannot be disclosed due to confidentiality.

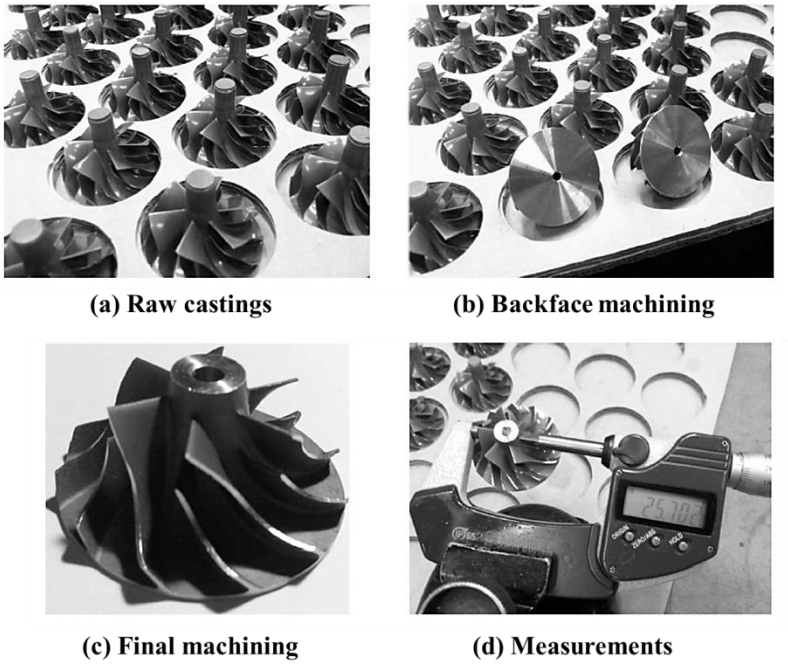

Figure 8 – Manufacturing of the DoE impellers for experimentation

machining of exit diameter has been carried out separately on a conventional lathe machine due to clamp size limitation. Finally, all the DoE impellers underwent a thorough inspection and measurements as shown in Fig. 8(d) in order to ensure precise manufacturing.

Experimental Setup

The impellers have been tested on the MTEE test bench, which is an advanced experimental setup for measuring turbocharger performance. Figure 9 shows the test bench without insulation. A natural gas burner is used to heat the compressed air, which is then supplied to the turbine through the turbine inlet pipe. A throttle valve located downstream of the compressor is used to regulate the mass flow during performance map measurement. Pre-heated oil at temperature of 100^{o}C and pressure of 3.5bar is pumped in the bearing housing for lubrication. Necessary insulation is used on the compressor inlet and outlet piping to minimize heat transfer from the hot turbine side. Furthermore, the turbine inlet temperature (TIT) has been maintained at 450K to minimize the heat

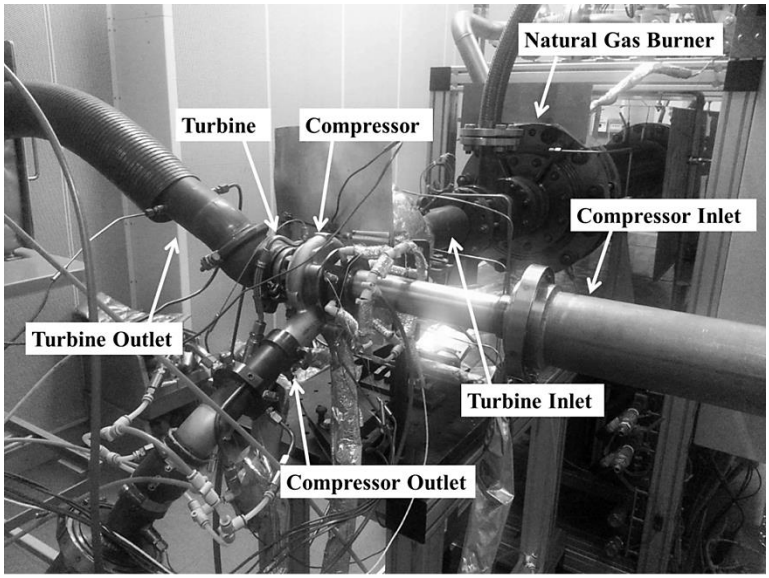

Figure 9 – MTEE turbocharger test bench

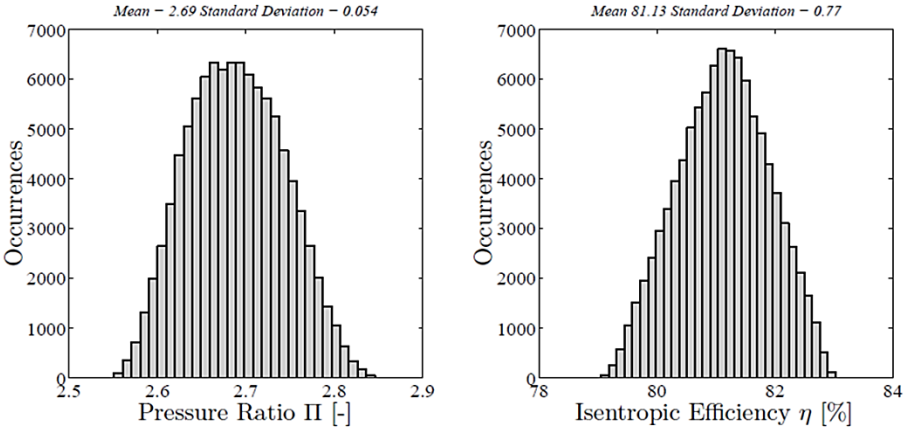

(a) Impeller performance variation predicted by the computational metamodel

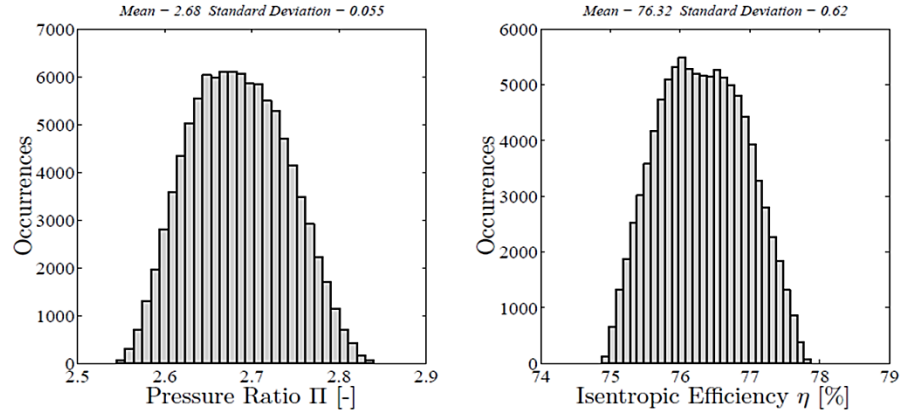

(b) Compressor performance variation predicted by the experimental metamodel

Figure 10 – Performance variation under manufacturing uncertainties predicted by the metamodel assisted Monte Carlo simulations.

transfer effects on compressor performance. Total temperatures and static pressures are measured at inlet and outlet stations of the turbocharger compressor, turbine and bearing housing. The sensors are placed at locations set according to MTEE measurement standards based on recommendations from the International Organization for Standardization (ISO). The 32 DoE impellers are installed one by one for each test on a single bearing housing. All the tests have been performed at the best-efficiency point and corrected to ISA ambient temperature and pressure of 288.15K and 101.325kPa, respectively.

Metamodel Construction and Evaluation

The experimental DoE responses for the compressor pressure ratio and isentropic efficiency have been fitted with quadratic response surfaces, which act as metamodels to predict the compressor performance at new observations. To check the usefulness of the metamodels in predicting the correct responses, the coefficient of determination R^2 and its adjusted form R^2_{adj} have been calculated. For the 32 impeller designs, the response surface for the pressure ratio resulted in R^2 and R^2_{adj} of 0.987 and 0.938, respectively, while for the impeller efficiency response surface, R^2 and R^2_{adj} are 0.985 and 0.931, respectively are achieved. The response surface models show a good fit, since R^2 and R^2_{adj} lie in a satisfactory range of 0.9-1.0. Nonetheless, the model fit for compressor isentropic efficiency is lower than the model fit for compressor pressure ratio.

Manufacturing Uncertainty Quantification

It is important to mention that the operating tip-clearance did not reduce to approximately 6% of tip height b_2 at the best-efficiency operating point. Following a sensitivity analysis using the test

data, the variation in tip-clearance between steady-state and operating turbocharger rotational speeds was found to be marginal during the tests, thus invalidating the nominal tip-clearance values used in the computational evaluations. To resolve this contradiction, the compressor performance has been extrapolated with the experimental metamodels corresponding to the nominal operating tip-clearance used in the computational evaluations. Furthermore, since the overall compressor stage performance is measured by the MTEE test bench, the relative change in performance has been considered for a suitable comparison between the computational and experimental outcomes.

For uncertainty propagation, a total of hundred thousand uniformly distributed Monte Carlo samples within the deviation ranges (now assumed as tolerances) defined in Table 4 have been evaluated using the experimental metamodels. For a comparison, similar Monte Carlo simulation using the computational metamodel has also been performed. Figure 10 presents the probability distributions, along with the statistical data produced by the computational and experimental metamodel based Monte Carlo simulations. As expected, the pressure ratio variation is closely predicted by the computational and experimental response surface models, where both are having comparable probability distributions and standard deviations. In comparison, the correspondence between the computational and experimental results for isentropic efficiency is rather satisfactory.

CONCLUSIONS

Comprehensive manufacturing uncertainty quantification for a micro centrifugal compressor impeller belonging to an automotive turbocharger has been carried out using computational and experimental methods. A versatile selection of engineering models has been used, which have been properly assessed, integrated and applied as a unit. As a result, the impeller shroud profile has been identified as the most critical geometric parameter. Deviations introduced in the impeller shroud profile due to inherent manufacturing uncertainties during trimming operation influence the tip-clearances. Accordingly, a strict tolerance has to be defined for the impeller shroud profile to regulate these dimensional deviations and the resulting performance variation.

Few discrepancies have been found mainly due to the differences in nominal tip-clearances at steady-state and operating turbocharger. In addition, the measurement uncertainties in the test bench are also contributing to the overall inconsistency found between the computational and experimental evaluations. Subsequently, these differences have been translated into the disagreements in the metamodel assisted computational and experimental analysis of isentropic efficiency. However, the experimental outcomes, although extrapolated, have given a good and valuable validation to the computational methods applied for the manufacturing uncertainty quantification of a turbocharger compressor impeller.

REFERENCES

R.S. Bunker, (2009), The Effects of Manufacturing Tolerances on Gas Turbine Cooling, ASME Journal of Turbomachinery, Vol. 131, P 1 – 11.

V.E. Gazron, D. L. Darmofal, (2003), Impact of Geometric Variability on Axial Compressor Performance", ASME Journal of Turbomachinery, Vol. 125, P 692 – 703.

N. Lecerf, D. Jeannel, A. Laude, (2003), A Robust Design Methodology for High-Pressure Compressor Throughflow Optimization, Proceedings of the ASME Turbo Expo 2003, Atlanta, Georgia, USA, GT2003-38264.

D. Bestle, P. M. Flassig, A. K. Dutta, (2011), Robust Design of Compressor Blades in the Presence of Manufacturing Noise, Proceedings of European Turbomachinery Conference ETC9, 2011, Istanbul, Turkey.

A. Kumar, P. B. Nair, A. J. Keane, S. Shahpar, (2008), Robust Design using Bayesian Monte Carlo, Int. J. Numer. Meth. Engng 2008, Vol 73, P 1497 – 1517.

T. Sotome, S. Sakoda, (2007), Development of Manufacturing Technology for Precision Compressor Wheel Castings for Turbochargers, Technical Review 32, Castings and Forging Division, Furukawa-Sky Aluminum, P. 56 - 60.

J. E. Hurtado, A. H. Barbat, (1998), Monte Carlo Techniques in Computational Stochastic Mechanics, Archives of Computational Methods in Engineering, Vol. 5, P. 3-30.

M. Olivero, A. Javed, R. Pecnik, J. P. van Buijtenen, (2011), Study of Tip-Clearance Effects in the Centrifugal Compressor of a Micro Turbine by Means of Numerical Simulations, Proceedings of International Gas Turbine Congress, Osaka, Japan.

S. Shahpar, (2004), Design of Experiment, Screening and Response Surface Modeling to Minimize the Design Cycle Time, Optimization Methods & Tools for Multi-criteria/Multidisciplinary Design, Lecture Series 2004-07, Von Karman Institute, Brussels, Belgium.

A. J. Keane, P. B. Nair, (2005), Computational Approaches for Aerospace Design - The Pursuit of Excellence, John Wiley and Sons Ltd.

F. R. Menter, (1993), Zonal Two-Equations k-ω Turbulence Models for Aerodynamic Flows, AIAA 93-2906, Proceedings of 24th Fluid Dynamics Conference, July 6-9 1993, Orlando, Florida.

R. H. Meyers, D. C. Montgomery, (1995), Response Surface Methodology: Process and Product Optimization Using Designed Experiments, Wiley, New York.